Applied Catalysis B: Environmental 150–151 (2014) 532–543

Contents lists available at ScienceDirect

Applied Catalysis B: Environmental

journal homepage: www.elsevier.com/locate/apcatb

Selective catalytic reduction of nitric oxide with ammonia over zirconium-doped copper/ZSM-5 catalysts

Feng Bin, Chonglin Song*, Gang Lv, Jinou Song, Shaohua Wu, Xiaodong Li

State Key Laboratory of Engines, Tianjin University, Weijin Road 92, Tianjin 300072, PR China

ARTICLE INFO

Article history:
Received 8 June 2013
Received in revised form
27 December 2013
Accepted 30 December 2013
Available online 7 January 2014

Keywords:
Selective catalytic reduction
Nitric oxide
Copper/ZSM-5
Zirconium doping

ABSTRACT

Selective catalytic reduction (SCR) of NO by NH_3 over a series of Cu-Zr/ZSM-5 catalysts with different zirconium loadings was studied to evaluate the correlation between structural characteristics and performance of the catalysts. The Cu-Zr/ZSM-5 catalysts exhibited nearly 100% NO conversion over a wide temperature range (167–452 °C), which is markedly superior to those of Cu/ZSM-5 (197–404 °C) and conventional V-W/TiO_2 catalyst (320–450 °C) and within the range of exhaust temperatures of diesel engines. Moreover, the zirconium enhances the sulfur tolerance of the catalysts. The effects of zirconium addition were investigated in detail by N_2 adsorption, X-ray diffraction (XRD), scanning electron microscopy (SEM), transmission electron microscopy (TEM), X-ray photoelectron spectroscopy (XPS), temperature-programmed desorption of NH_3 (NH_3-TPD), temperature-programmed reduction by hydrogen (H_2-TPR), oxygen storage capacity (OSC), electron paramagnetic resonance (EPR), ultraviolet–visible diffuse reflectance spectra (UV–vis DR) and *in situ* diffuse reflectance Fourier transform (DRIFT) spectroscopy. The TEM, XRD and UV–vis DR results showed that addition of zirconium increased the dispersion of copper and prevented its crystallization. The XPS results demonstrated that the introduction of zirconium enhanced the enrichment of copper species on the surfaces of ZSM-5 grains. Addition of zirconium improved the redox properties of the Cu-Zr/ZSM-5 catalysts, which arose from the higher valence of copper and mobility of lattice oxygen than those of Cu/ZSM-5 catalyst. The DRIFT results confirmed that the SCR reaction over Cu-Zr/ZSM-5 catalysts mainly followed the Langmuir–Hinshelwood mechanism; *i.e.*, reaction of activated NO_x species with activated NH_3 species. The Cu-Zr/ZSM-5 catalysts were able to accelerate the oxidation of NO to NO_2 in the presence of oxygen. Compared with Cu/ZSM-5 catalyst, the Cu-Zr/ZSM-5 catalysts caused the amount of $-NO_2$ species after $NO + O_2$ adsorption to increase, resulting in the temperature range for optimum NO_x reduction (>95%) extending to lower temperature.

1. Introduction

Selective catalytic reduction (SCR) of NO_x with NH_3 is currently considered the most efficient technology for NO_x removal from stationary sources. In widespread use for this process is titania-supported V_2O_5–WO_3, which exhibits optimum performance in a narrow temperature window (300–400 °C) [1]. Recently, this technology has been widely employed in mobile diesel engines in Europe to meet impending emission standards. However, it is difficult to achieve effective NO_x reduction with existing titania-based catalysts in diesel engines because the temperature of the exhaust tailpipe typically varies in the range of 200–400 °C [2]. In this case, transition metal-containing zeolites, particularly Cu/ZSM-5, appear to be the most promising candidates. Isolated copper ions and copper oxides have been identified as the active sites for NO_x reduction in such systems, with turnover frequency decreasing in the order: isolated copper ions > small CuO_x clusters > large CuO_x clusters > CuO particles [3,4]. With respect to monometallic copper-loaded catalysts, it is difficult to enhance the activity for NO_x reduction simply by increasing the copper content. This is because a high copper loading ratio inevitably leads to agglomeration of the copper species and formation of large copper oxide particles [5]. Increasing the copper content also causes the active temperature window to narrow slightly because oxidation of NH_3 is induced by the CuO particles. It has been determined that the optimal copper content in such systems is within the range of 3–4 wt% [6].

Zirconia is well known as an effective promoter for metal-based catalysts, and acts as a phase stabilizer to increase the dispersion and stability of the active metal through strong metal-support interactions [7]. Although zirconium-containing multi-metal catalysts, such as $Cu/Ce_xZr_{1-x}O_2$ [8], $K_4Zr_5O_{12}$ [9] and Co-Ba-K/ZrO_2 [10], are widely used for soot oxidation in diesel engine exhaust, their application in the SCR of NO_x with NH_3 are scare. Herein, we have developed the zirconium-promoting Cu/ZSM-5 catalysts. In

* Corresponding author. Tel.: +86 22 27406840x8020; fax: +86 22 27403750.
E-mail address: songchonglin@tju.edu.cn (C. Song).

0926-3373/$ – see front matter © 2014 Elsevier B.V. All rights reserved.
http://dx.doi.org/10.1016/j.apcatb.2013.12.052

terms of the oxygen storage, surface acid, reducibility, structures and chemical valences of copper, the present work is to comprehensively explore the promotional effect of zirconium addition on the activity of Cu-Zr/ZSM-5 catalysts. Based on the characterization results and the catalytic performances, potential reaction mechanism is proposed and discussed in detail.

2. Experimental

2.1. Catalyst preparation

A series of Cu-Zr/ZSM-5 catalysts were prepared by an ion-exchange technique. H/ZSM-5 with an atomic Si/Al ratio of 25 and crystallinity of 100% was supplied by Nankai University, Tianjin, PR China. Appropriate amounts of copper nitrate and zirconium nitrate were dissolved in deionized water and mixed with 0.5 g of H/ZSM-5 (Si:Al = 25:1). The resulting solution was stirred at 80 °C for 24 h. After drying by evaporation, the sample was calcined at 550 °C for 4 h. The contents of copper and zirconium in each calcined catalyst were determined by atomic absorption spectroscopy (AAS) using a Perkin-Elmer AAnalyst 300 spectrometer. The copper content of the Cu-Zr/ZSM-5 (CuZr-Z) catalysts was fixed at 2.2 wt%, and zirconium contents of 0.3, 0.5, 1.1 and 2.2 wt% were used, giving catalysts that are designated CuZr1-Z, CuZr2-Z, CuZr3-Z and CuZr4-Z, respectively. For comparison, 2.2 wt% Cu/ZSM-5 (Cu-Z) was also prepared as described above and a conventional 3 wt% V_2O_5–8 wt% WO_3/TiO_2 (V-W/TiO_2) catalyst was prepared by the impregnation method. WO_3/TiO_2 with a loading of tungsten of 8 wt% was prepared by adding TiO_2 to a vigorously stirred solution of ammonium tungstate. The obtained slurry was stirred for 2 h at room temperature, and then heated to dryness at 80 °C under continuous stirring. The obtained solid was heated in an oven at 110 °C overnight and was subsequently calcined for 3 h at 550 °C in air. The catalyst with 3 wt% loading of V_2O_5 was synthesized by adding WO_3/TiO_2 powder to a blue solution prepared by reacting ammonium metavanadate with oxalic acid. The resulting slurry was submitted to the evaporation, drying and calcination process described above to give the V-W/TiO_2 catalyst.

2.2. Catalyst characterization

N_2 adsorption isotherms were measured at −196 °C on a NOVA-2000 analyzer (Quantachrome, Boynton Beach, FL, USA). Before measurement, samples were evacuated for 10 h at 300 °C. The standard Brunauer–Emmett–Teller (BET) method was used to calculate the specific surface area of each sample from adsorption data. The morphology and phase purity of the samples were acquired from scanning electron microscope (SEM, Hitachi S4800) and transmission electron microscope (TEM, PHILIPS Tecnai G^2 F20) observations, coupled with a Oxford-1NCA EDX detector. The crystalline phase of each sample was determined by powder X-ray diffraction (XRD) using a Rigaku D/MAC/max 2500v/pc diffractometer with Cu Kα radiation (40 kV, 200 mA, λ = 1.5418 Å). X-ray photoelectron spectra (XPS) were recorded on a Perkin-Elmer PHI-1600 ESCA spectrometer using a Mg Kα X-ray source. The electron paramagnetic resonance (EPR) spectroscopic measurements were performed in a Bruker Model A320 equipment at 300 and 120 K with the X-band (9.78 GHz). Ultraviolet–visible diffuse reflectance spectra (UV–vis DR) were measured on a Hitachi U-4100 UV–vis spectrophotometer with an integration sphere diffuse reflectance attachment. Powder samples were loaded into a transparent quartz cell and were measured in the region of 200–800 nm at room temperature. Temperature-programmed desorption of NH_3 (NH_3-TPD) testing was performed using a Micromeritics Autochem 2920 II analyzer with a thermal conductivity detector (TCD). After pretreatment at 300 °C under flowing helium (50 mL/min) for 1 h, each sample (100 mg) was cooled to 50 °C, and then adsorbed to saturation by pulses of ammonia for 0.5 h. Ammonia physically adsorbed on the catalyst was removed by flushing the sample with helium (50 mL/min) for 1 h at the adsorption temperature. Thermal desorption of ammonia was carried out in the temperature range of 50–700 °C increasing at a rate of 10 °C/min. Temperature-programmed reduction with hydrogen (H_2-TPR) experiments were performed with a Micromeritics 2920 II analyzer. For the analysis, each sample (100 mg) was pretreated in 20 vol% oxygen at 550 °C for 30 min. After cooling to 100 °C, H_2-TPR measurements were recorded in 10 vol% H_2 (50 mL/min) with a heating rate of 10 °C/min and a final temperature of 500 °C. Oxygen storage capacity (OSC) measurements were also carried out on the Micromeritics Autochem 2920 II analyzer. Each sample (100 mg) was reduced at 550 °C for 1 h in H_2 (10 mL/min), then cooled to 400 °C and purged continuously with He (30 mL/min) for 20 min. Oxygen was injected into the sample until no oxygen consumption could be detected by the TCD. Total OSC was calculated by integrating the O_2 consumed (μmol [O] g^{-1}). *In situ* diffuse reflectance Fourier transform (DRIFT) measurements were obtained on a Bruker V70 FTIR spectrometer equipped with a mercury cadmium telluride (MCT) detector. Before recording spectra, the sample disk placed in the DRIFT cell with a CaF_2 window was pretreated in a flow of Ar at 500 °C and subsequently cooled to 170 °C. An adsorption temperature of 170 °C was chosen to minimize the reaction rate so that the concentration of surface species was enhanced to a detectable level. The background spectrum of the pretreated sample surface was measured for spectral correction. The reactant gas mixture of NO (1.0 vol%), O_2 (5 vol%) and NH_3 (1 vol%) with Ar as the balance was introduced into the DRIFT cell *via* separate mass flow controllers and the flow rate was set at 40 mL/min. In these experiments, FT-IR spectra were recorded (64-scan accumulation and 4 cm^{-1} resolution) in succession at 1-min intervals.

2.3. Catalytic activity test

Catalytic experiments were performed at atmospheric pressure in a flow-type apparatus designed for continuous operation. Granulated catalyst (0.5 g) was packed into a fixed-bed reactor made of a quartz tube with an internal diameter of 10 mm. A K-type thermocouple was located inside the catalyst bed to monitor reaction temperature. The SCR of NO by NH_3 was carried out across the temperature range 50–600 °C, and the feed gas (1000 ppm NO, 1000 ppm NH_3, and 10 vol% O_2 with N_2 as the balance; space velocity (SV) of 100,000 h^{-1}) was metered using calibrated electronic mass flow controllers. In some tests, 5 vol% H_2O, obtained by helium passing through a saturator with deionized water, and 100 ppm of SO_2 were added to the used feed gas respectively. To study the effects of the catalysts on non-selective oxidation of NH_3, the catalytic activity for NH_3 oxidation was also examined using feed gas consisting of 1000 ppm NH_3, 10 vol% O_2 and the balance N_2. An online multi-component measurement system (AVL SESAM-FTIR) was used to monitor the effluent NO, NO_2, N_2O and NH_3. The concentration of H_2O and SO_2 were monitored by using the on-line quadrupole mass spectrometer (AMETEK, Dycor LC-D200).

3. Results and discussion

3.1. Catalytic performance

Fig. 1A shows the results for NO conversion in SCR reactions over V-W/TiO_2, Cu-Z and CuZr-Z catalysts as a function of temperature. The V-W/TiO_2 catalyst is inactive below 300 °C and NO reduction

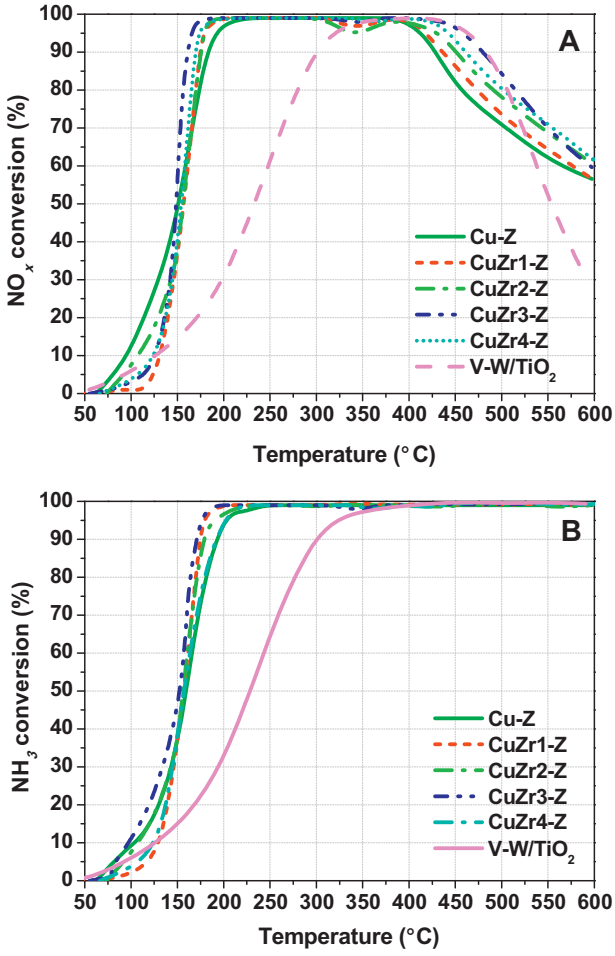

Fig. 1. SCR activity for NO_x (A) and NH_3 (B) conversions as a function of reaction temperature for V-W/TiO_2, Cu-Z and CuZr-Z catalysts. The standard deviations for the NO_x conversion are within the range of 0.8–2.1. Conditions: 1000 ppm NO, 1000 ppm NH_3, 10 vol% O_2 and N_2 to balance; space velocity: 100,000 h^{-1}; weight of catalyst: 0.5 g.

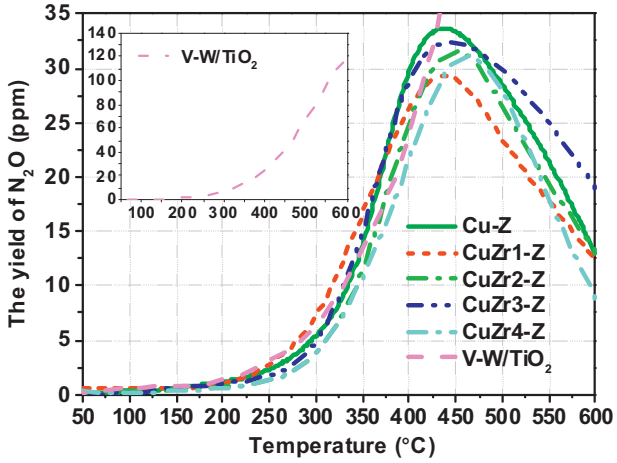

Fig. 2. Yield of N_2O during the SCR process as a function of reaction temperature for V-W/TiO_2, Cu-Z and CuZr-Z catalysts. The standard deviations for the yield of N_2O are within the range of 0.6–2.7. Conditions: 1000 ppm NO, 1000 ppm NH_3, 10 vol% O_2 and N_2 to balance; space velocity: 100,000 h^{-1}; weight of catalyst: 0.5 g.

higher than 95% is achieved within the range of 320–450 °C. Typical activity of the V-W/TiO_2 catalyst has been reported in literatures. Cha et al. [11] confirmed that the commercial V_2O_5-WO_3/TiO_2 material reaches the NO conversion levels of 94%, 100%, and 96% at 325, 350, and 375 °C, respectively. Lin et al. [12] found that the V_2O_5/TiO_2 catalyst exhibits a low-temperature activity for the NO conversion, whereas the active window is at 275–325 °C. According to Vargas et al. [13], the activity of erbium-containing V_2O_5-WO_3/TiO_2 catalyst is improved after aging, with NO conversion reaching 95% at 300–380 °C. In this work, Cu-Z exhibits excellent activity for SCR with NO conversion above 95% in the range of 197–404 °C. When appropriate amounts of zirconium are added to Cu/ZSM-5, the temperature range for efficient NO reduction (>95%) extends to both lower and higher temperature; *i.e.*, the active window widens. Among the Cu-Zr/ZSM-5 catalysts tested, the CuZr3-Z sample exhibits the highest catalytic activity with a temperature range for 95% NO removal of 167–452 °C. The temperature ranges in which it is possible to achieve the same level of NO conversion for the other three zirconium-doped catalysts are 182–412 °C (CuZr1-Z), 178–424 °C (CuZr2-Z) and 176–437 °C (CuZr4-Z). The SCR activities of the catalysts follow the order: V-W/TiO_2 < Cu-Z < CuZr1-Z < CuZr2-Z < CuZr4-Z < CuZr3-Z. Further addition of zirconium (>2.2 wt%) decreases the activity of the catalyst. According to these results, it does not make sense to increase the zirconium loading above 2.2 wt% for SCR.

The NH_3 conversion results during SCR are plotted in Fig. 1B. The conversion of NH_3 by all of the catalysts increases monotonically with operating temperature and reaches 100% at 436 °C for V-W/TiO_2 and at above 200 °C for Cu-Z and CuZr-Z catalysts. Combined with the NO conversion results for the temperature range <450 °C for V-W/TiO_2, and <200 °C for Cu-Z and CuZr-Z catalysts, the conversion of NH_3 is close to that of NO, suggesting that most NH_3 is involved in the SCR reaction. In the temperature range >450 °C for V-W/TiO_2, and >200 °C for Cu-Z and CuZr-Z catalysts, the observed decrease of NO conversion (shown in Fig. 1A) and complete NH_3 conversion reveal that there is competition between the reduction of NO by NH_3 and direct oxidation of NH_3 into NO or N_2O.

We found that NO_2 and N_2O are produced as byproducts during SCR. The concentration of NO_2 is below 3 ppm during SCR on all of the catalysts. Fig. 2 indicates that the formation of N_2O by the V-W/TiO_2 catalyst increases steadily with temperature, reaching a concentration of 120 ppm at 600 °C. This result is consistent with that for the NH_3-SCR processes shown in Fig. 1, where a significant decrease in NO conversion is found between 400 and 600 °C for the V-W/TiO_2 catalyst. The increased amount of N_2O produced arises from direct oxidation of NH_3 *via* the reaction $2NH_3 + 2O_2 \rightarrow N_2O + 3H_2O$. In contrast, the ZSM-5-based catalysts inhibit N_2O formation during SCR compared with the V-W/TiO_2 catalyst. N_2O formation by the Cu-Zr/ZSM-5 catalysts increases and then decreases as the temperature increases, with the maximum values (<35 ppm) observed between 435 and 463 °C (Fig. 2).

To shed light on the effects of V-W/TiO_2, Cu-Z and CuZr-Z catalysts on the non-selective oxidation of NH_3, the activity of these catalysts for the oxidation of NH_3 in the presence of oxygen was examined. Fig. 3 reveals that the oxidation of NH_3 over V-W/TiO_2 catalyst begins at about 200 °C and increases monotonically with temperature, reaching 91% conversion at 600 °C. Compared with the V-W/TiO_2 catalyst, the Cu-Z catalyst promotes the non-selective NH_3 oxidation at temperature < 500 °C but resists NH_3 oxidation effectively at temperature > 500 °C. This inhibition of non-selective NH_3 oxidation is much more pronounced for the CuZr-Z catalysts than that for Cu-Z. The NH_3 oxidation decreases initially with increasing zirconium content from 0 to 1.1 wt%, then considerably increases with further raising zirconium content to 2.2 wt%.

Overall, the Cu-Z and CuZr-Z catalysts show potential for both the SCR of NO to N_2 and the non-selective catalytic oxidation of NH_3. However, the SCR activity of the catalysts is higher than that of non-selective NH_3 oxidation, which is attributed to the higher reactivity of NH_3 with NO than with O_2 [14]. The decrease of NO

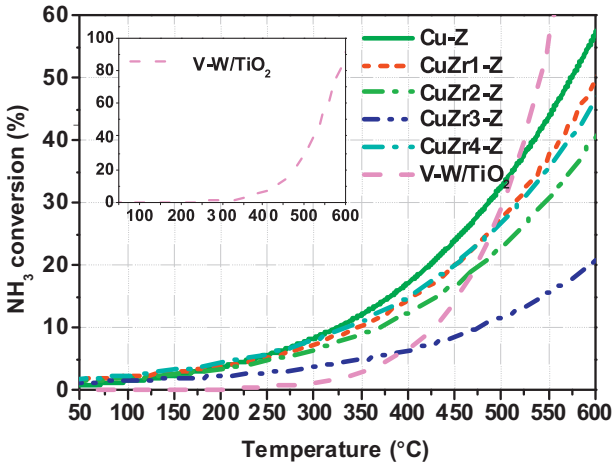

Fig. 3. Direct NH_3 oxidation as a function of reaction temperature for V-W/TiO_2, Cu-Z and CuZr-Z catalysts. The standard deviations for direct NH_3 oxidation are within the range of 0.8–3.5. Conditions: 1000 ppm NH_3, 10 vol% O_2 and N_2 to balance; space velocity: 100,000 h^{-1}; weight of catalyst: 0.5 g.

conversion at temperatures >400 °C is assigned to the non-selective oxidation of NH_3 during the SCR process.

3.2. Vapour and sulfur tolerance of catalysts

The vapour and sulfur deactivation characteristics of V-W/TiO_2, Cu-Z and CuZr3-Z catalysts are shown in Fig. 4. Before adding H_2O or SO_2, the SCR over these catalysts are stabilized during a 100 h-operation at 300 °C, as shown in Fig. 4A. It is found from Fig. 4B that the NO conversion under the dry condition is higher than that under the wet condition on all the catalysts. The decrease of SCR activity is caused by the competitive adsorption of H_2O and the reactants, *i.e.* NO and/or NH_3. However, the activities of catalysts are almost restored to its original level after cutting off the injection of H_2O. When 100 ppm SO_2 is added into the reactants, the SCR activities for both V-W/TiO_2 and Cu-Z remarkably decrease as compared to that for CuZr3-Z (Fig. 4C), and the deactivation of SO_2 is not recovered for all the catalysts. The poisoning effect of SO_2 on catalyst takes place mainly via the following approaches: The ammonium sulfate deposited on the catalyst surface covers available active

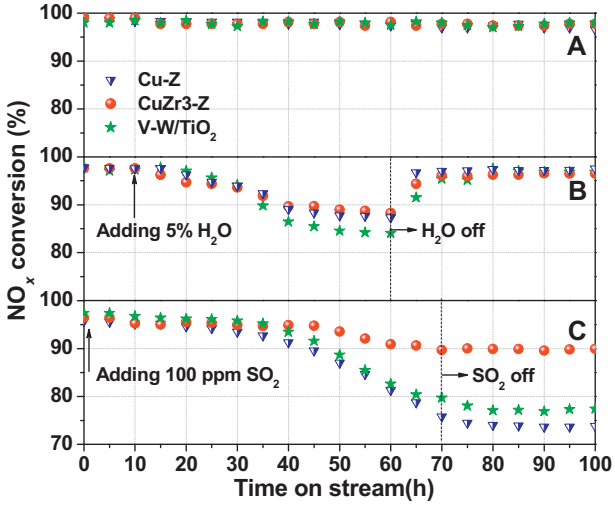

Fig. 4. Effect of SO_2 and H_2O on the SCR of NO_x with NH_3 over V-W/TiO_2, Cu-Z and CuZr3-Z catalysts. Conditions: 1000 ppm NO, 1000 ppm NH_3, 10 vol% O_2, 5 vol% H_2O (B), 100 ppm SO_2 (C) and N_2 to balance; space velocity: 100,000 h^{-1}; weight of catalyst: 0.5 g.

Table 1
BET surface area and micropore volume of pure ZSM-5, Mn/ZSM-5 and MnZr/ZSM-5 catalysts.

Sample	BET surface area ($m^2\ g^{-1}$)	Micropore volume ($cm^3\ g^{-1}$)
Pure ZSM-5	376	0.15
Cu-Z	362	0.14
CuZr1-Z	357	0.13
CuZr2-Z	345	0.13
CuZr3-Z	327	0.12
CuZr4-Z	304	0.11

sites, blocks zeolite channels and sulfates the active components, resulting in inactivation [15,16]. The excellent sulfur tolerance of CuZr3-Z is probably attributed to the introduction of zirconium oxide, which is most likely to act as a sacrificial sulfidation site, taking the sulfur species away from the active components [17]. Bazin et al. [18] reported that the addition of zirconium appeared to decrease the mobility of surface sulfates towards the bulk of the sample, hindering sulfation.

3.3. Structure and morphology

The Cu-Z and CuZr-Z catalysts, together with the ZSM-5 support, were characterized by N_2 adsorption–desorption measurements. Table 1 shows that doping ZSM-5 with copper and/or zirconium leads to a decrease in BET surface area and micropore volume, from 376 m^2g^{-1} and 0.15 cm^3g^{-1}, respectively, for ZSM-5 to 362 m^2g^{-1} and 0.14 cm^3g^{-1}, respectively, for Cu-Z, to 304 m^2g^{-1} and 0.11 cm^3g^{-1}, respectively, for CuZr4-Z. The reason for this may be that copper and zirconium species cover the external surface of ZSM-5, blocking a number of zeolite channels, and impeding entry of N_2 into the pores. XRD patterns (Fig. 5) of pure ZSM-5 and samples doped with copper and/or zirconium are characterized by peaks at $2\theta = 7.9°$, 8.8°, 23.1° and 23.8°, which represent the (0 1 1), (0 2 0), (0 5 1) and (0 3 3) planes of their crystal structures, respectively. The intensities of the principal diffraction peaks of ZSM-5 decrease remarkably with increasing zirconium content. No

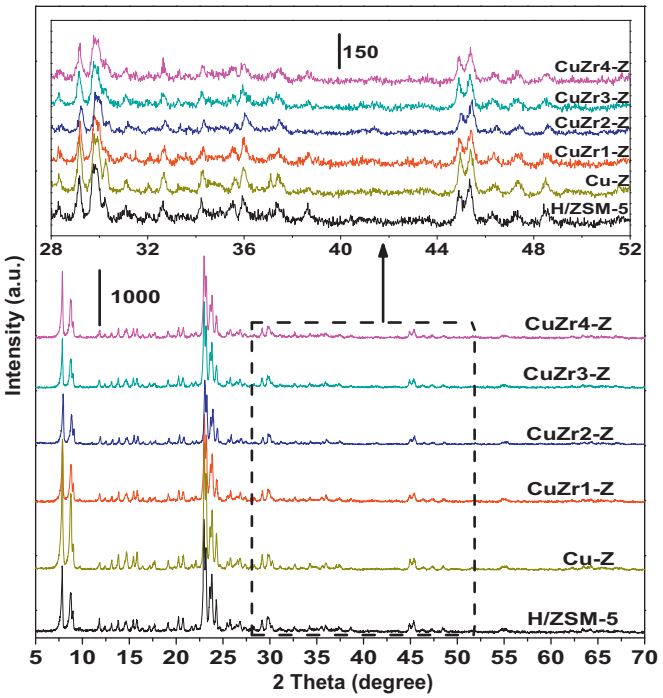

Fig. 5. Wide-angle XRD patterns of pure ZSM-5, Cu-Z and CuZr-Z catalysts after calcination in air at 550 °C for 3 h.

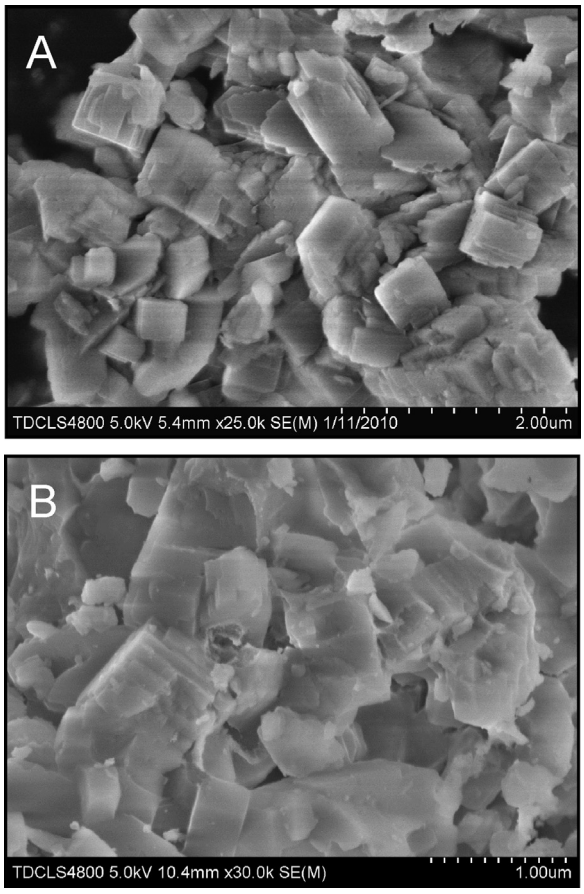

Fig. 6. SEM images for (A) Cu-Z and (B) CuZr4-Z catalysts.

diffraction peaks attributed to either copper or zirconium oxides are observed, which suggests that the copper and zirconium species formed are in the nanometer size range and are well dispersed on the ZSM-5 support.

Pure ZSM-5 sample is commonly composed of irregularly localized, bright polycrystalline aggregates with distinct edges. The SEM images in Fig. 6 show that the morphology of ZSM-5 is virtually unchanged after incorporation of copper and zirconium. However, the surface of the ZSM-5 grains is coated with a layer when the zirconium is present. TEM analysis (Fig. 7A) revealed that the copper species in the Cu-Z sample are dispersed uniformly, and that this degree of dispersion can be maintained until the zirconium content increases to 1.1 wt% for CuZr3-Z. For a zirconium content of 2.2 wt%, distinct darker spots (indicated as point 1 and 2 in Fig. 7B) are apparent. The EDX spectra of these particles indicate they are composed of copper, zirconium and oxygen-rich phases (Ni peaks arose from the supporting nickel grid). Moreover, an inhomogeneous distribution of copper and zirconium oxides (point 3, marked as an ellipse in Fig. 7B) suggests that a large fraction of the copper and zirconium oxide clusters are located on the outer surface of the ZSM-5 crystals.

3.4. XPS analysis

The chemical states and surface compositions of the elements in the different catalysts were characterized by XPS. The Cu 2p spectrum of Cu-Z (Fig. 8A) shows two main peaks that are attributed to Cu $2p_{3/2}$ and Cu $2p_{1/2}$ at about 933.1 and 953.3 eV, respectively. For the Cu-Z sample, the Cu $2p_{3/2}$ peaks show considerable asymmetry. Peak deconvolution and fitting to experimental data (Fig. 8A) indicate that the Cu $2p_{3/2}$ peak could be fitted well by two peaks corresponding to the chemical states of Cu^+ at 932.5 eV with a shake-up peak located at 936–945 eV and Cu^{2+} at 933.8 eV. After doping with zirconium, the binding energy of Cu $2p_{3/2}$ shifted to the slightly higher value (*e.g.*, CuZr4-Z), confirming that some Cu^+ is oxidized to Cu^{2+}. The area ratios of Cu^{2+}/Cu^+ calculated from the XPS data are shown in Table 2. The Cu^{2+}/Cu^+ ratio is 0.92 for the Cu-Z sample and increases with zirconium content. The highest Cu^{2+}/Cu^+ ratio is 1.73 for the CuZr4-Z catalyst.

The O 1s XPS spectra of pure ZSM-5, Cu-Z and CuZr4-Z catalysts are shown in Fig. 8B. These samples exhibit two O 1s XPS peaks. The one at lower binding energy (~530.2 eV) is related to lattice oxygen from copper and zirconium oxides (Oo), and the other at higher binding energy (~532.6 eV) corresponds to regular lattice oxygen from the ZSM-5 zeolite structure (Oz) [19–21]. Because the XPS peaks of O 1s are not symmetric, they were deconvoluted to give the relative content of different oxygen species corresponding to low and high binding energies. When zirconium is introduced, the ratio of the area of lattice oxygen of the metal oxides to that of ZSM-5 (Oo/Oz) increases regularly with zirconium content, as shown in Table 2. Considering that copper and zirconium oxides were not detected by XRD, they are well dispersed on the ZSM-5 support.

Elemental compositions were calculated from the areas of O 1s, Si 2p, Cu 2p, and Zr 3d peaks and are also shown in Table 2. The results confirm that the superficial copper content increases with zirconium loading ratio. XPS is a surface technique that preferentially detects species located on the surface of a sample (sampling depth is about 3–10 nm). Copper appears to become enriched on the surface of ZSM-5 grains, because the Cu/Si atomic ratios for the Cu-Z and CuZr-Z samples are considerably larger than those obtained from AAS and increase monotonically with zirconium content. In addition, the surface atomic ratio of Cu/Zr increases with zirconium content (Table 2). The enriched copper ions may interact with zirconium ions to cover the ZSM-5 grains.

Zr 3d spectra (Fig. 8C) of the CuZr4-Z samples exhibit doublets corresponding to Zr $3d_{3/2}$ at about 184.5 eV and Zr $3d_{5/2}$ at about 182.1 eV. Importantly, the binding energy of Zr $3d_{5/2}$ in the catalyst is higher than that of zirconium metal (180.0 eV), but lower than that of ZrO_2 (182.4 eV), which might be caused by strong interactions at the ZSM-5 surface involving charge transfer from copper to zirconium. The presence of more reduced zirconium species has been associated with a high population of oxygen vacancies in the ZrO_2 lattice [22]. Moreover, Wang et al. [23] observed zirconium cations with a lower binding energy than ZrO_2, who ascribed this to copper oxides located near oxygen vacancies on the surface of ZrO_2. Lead zirconate titanate oxides also showed similar behavior [24].

After SCR, the Cu $2p_{3/2}$ main line of the used CuZr4-Z catalyst is located at 932.9 eV (Fig. 8A), compared with 933.4 eV before the reaction, which corresponds to partial reduction of Cu^{2+} cations to Cu^+. The Zr 3d peak obtained for the CuZr4-Z catalyst shifted slightly to higher binding energy (Fig. 8C). The increase in binding energy confirms that the electron density on the zirconium species is slightly higher than before the reaction, but it is still lower than that of ZrO_2. It is possible that oxygen vacancies still exist on the catalyst surface after SCR.

3.5. EPR and UV-vis DR analysis

The hyperfine structure of isolated Cu^{2+} species can be characterized by EPR spectra, while Cu^+ and Zr^{4+} cations do not contribute to EPR. Therefore, EPR is an effective method to identifying isolated Cu^{2+} on Cu-zeolite catalysts. Fig. 9 depicts the EPR results of the Cu-Z and CuZr3-Z samples at 120 and 300 K. In these samples, copper species should be present as EPR active Cu^{2+} ions. However, hyperfine features are barely detectable, which is a

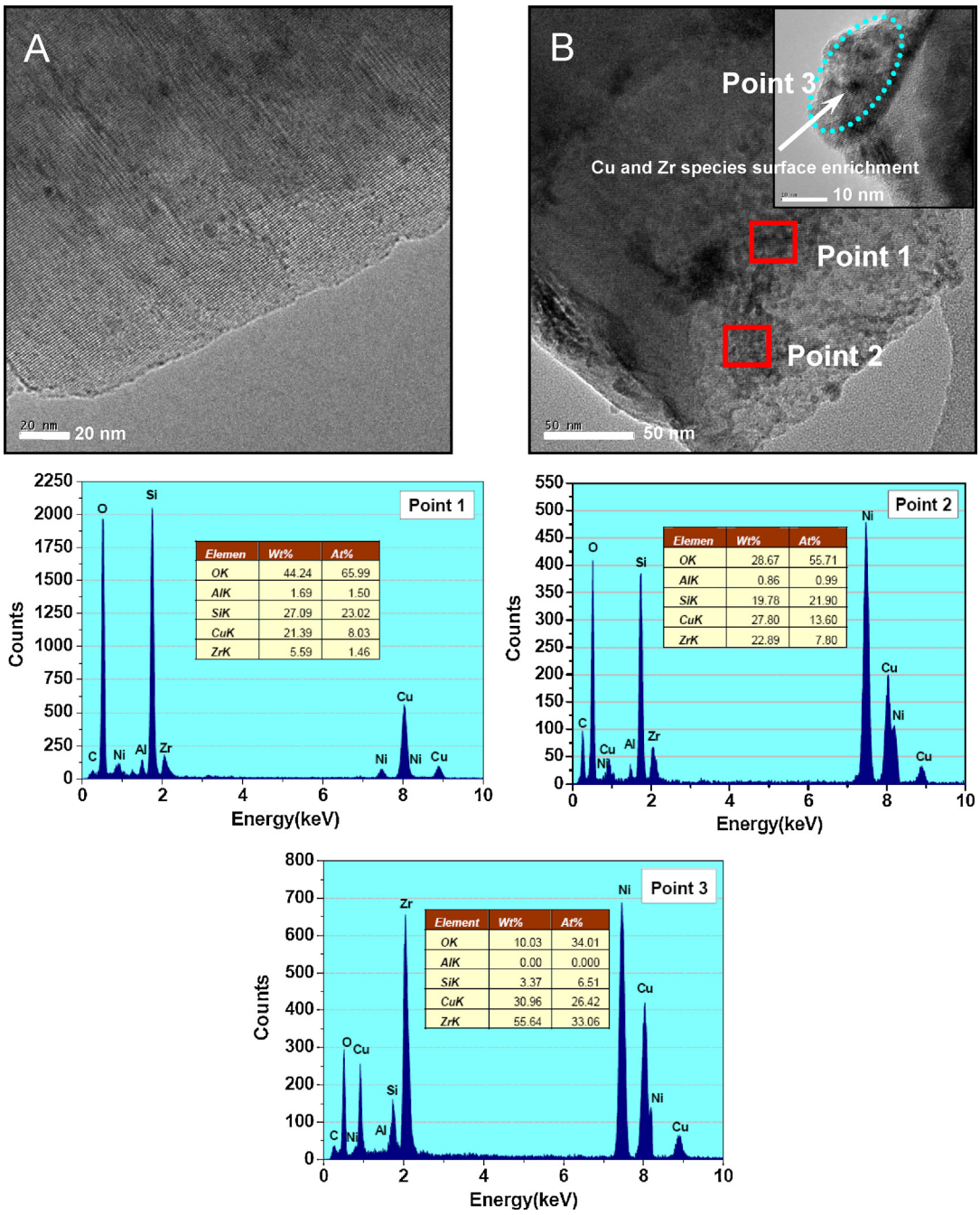

Fig. 7. TEM and EDX images for (A) Cu-Z and (B) CuZr4-Z catalysts. The nickel peaks in EDX spectra arise from the supporting nickel grid.

strong spin-lattice interaction at 300 K, resulting in broadening of EPR peaks. This behavior is presumably caused by a combination of facile Cu^{2+} ion mobility and strong dipolar interactions between Cu^{2+} ions [25]. In order to decrease Cu^{2+} ion mobility and allow only dipole-dipole interactions to be monitored, additional EPR measurements were performed at 120 K. The EPR spectra of Cu-Z and CuZr3-Z samples at 120 K are characterized by axial anisotropy of the g factor with a resolved hyperfine structure due to

Table 2
Surface compositions of Cu-Z and CuZr-Z catalysts derived from XPS analysis.

Sample	Surface element composition (at%)				Cu/Si		Zr/Si		Cu/Zr	Cu^{2+}/Cu^{+}	Oo/Oz
	O	Si	Cu	Zr	AAS	XPS	AAS	XPS	XPS		
Cu-Z	35.8	15.2	0.4	0	0.012	0.026	0	0	–	0.92	0
CuZr1-Z	31.6	15.7	0.8	1.3	0.012	0.051	0.001	0.083	0.62	1.17	0.04
CuZr2-Z	34.4	16.1	1.1	1.5	0.012	0.068	0.002	0.093	0.73	1.27	0.08
CuZr3-Z	35.8	16.3	1.3	1.8	0.012	0.080	0.004	0.110	0.72	1.49	0.12
CuZr4-Z	35.3	15.2	1.5	2.0	0.012	0.099	0.007	0.132	0.75	1.73	0.20

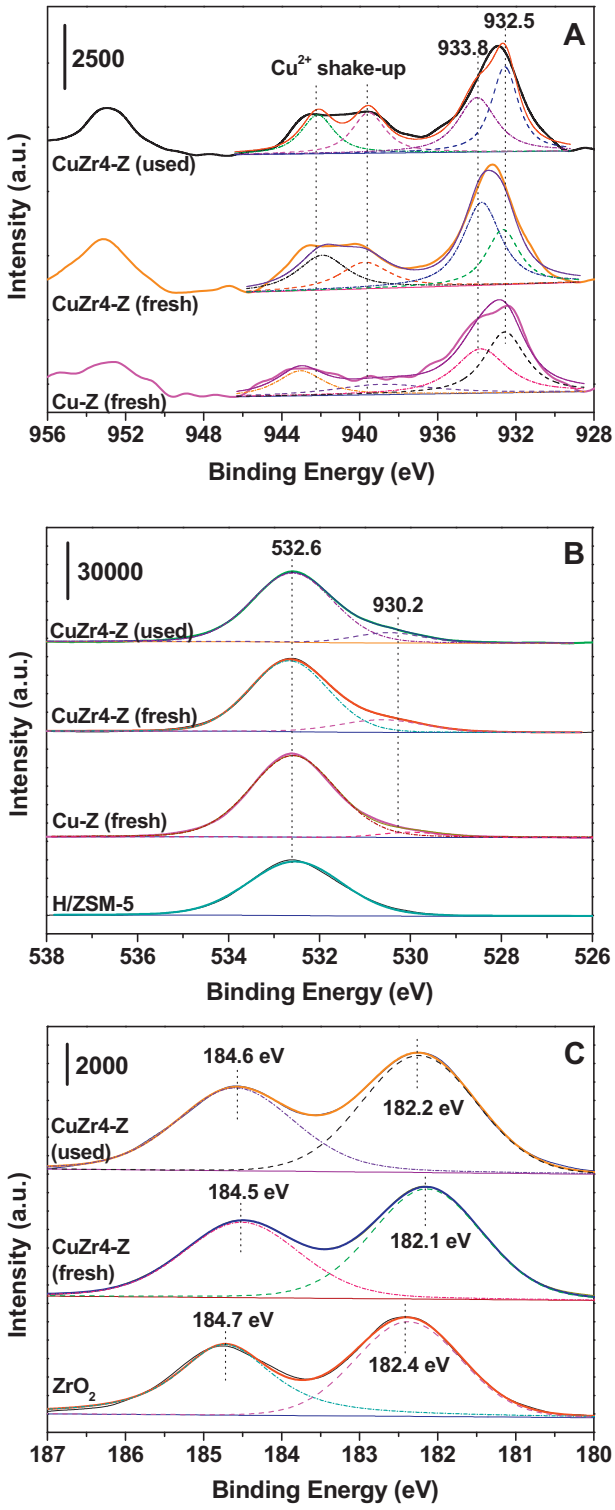

Fig. 8. XPS narrow spectra of Cu 2p (A) and O 1s (B) and Zr 3d (C) from the ZrO_2, pure ZSM-5, Cu-Z and CuZr4-Z catalysts. Crude line: original data; Smooth line: fitting line.

isolated Cu^{2+} species. Each spectrum exhibits four hyperfine features ($m_I = -3/2, -1/2, +1/2, +3/2$) in the low field region of the spectrum, characteristic of the copper nucleus with $I = 3/2$. The EPR parameters ($g_{//} = 2.39$, $g_{\perp} = 2.07$, $A_{//} = 138$ G) correspond to isolated Cu^{2+} ions with tetragonally distorted octahedral coordination of oxygen-containing ligands [26]. Although the EPR spectra of Cu-Z and CuZr3-Z are located similarly, there are subtle differences in

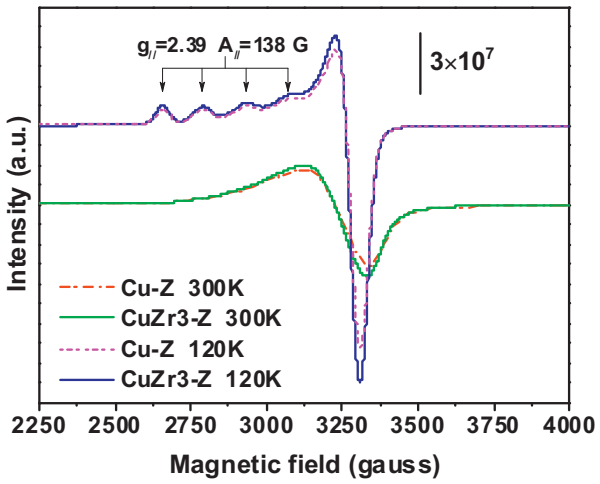

Fig. 9. EPR spectra of Cu-Z and CuZr3-Z catalysts at 300 K and 120 K.

intensity of the low field hyperfine. The intensity of Cu^{2+} signals in the EPR spectra increases after the zirconium introduction, demonstrating the increase of Cu^{2+} concentration. UV–vis DR spectroscopy is applied to understand the nature and coordination of copper oxide species in the samples. As shown in Fig. 10, the Cu-Z sample displays two absorption bands at 206 and 260 nm, and a broad and weak band at 600–800 nm. The absorption band at 206 and 260 nm can be assigned to oxygen-to-metal charge-transfer related to the Cu^{+} or Cu^{2+} ions doped and stabilized in the framework of zeolite [27]. The band centered at 260 nm appears asymmetry, and the shoulder between 300 and 450 nm corresponds to the transitions of Cu^{2+} in tetragonal oxygen configuration [28], which can be assigned to the formation of well dispersed CuO_x clusters on the surface of ZSM-5 grains. The absorption band between 600 and 800 nm is related to the transitions of Cu^{2+} in octahedral oxygen configuration more or less tetragonally distorted, corresponding to the CuO phase [29]. These results are basically in agreement with that of EPR analysis. The zirconium introduction enhances the band at 206 nm since ZrO_2 nanoparticles have main absorption in UV region [30]. The reduction of visible light absorption (600–800 nm), together with the band at 260 nm broadening after the zirconium addition, indicates the enhancement of copper oxide dispersion.

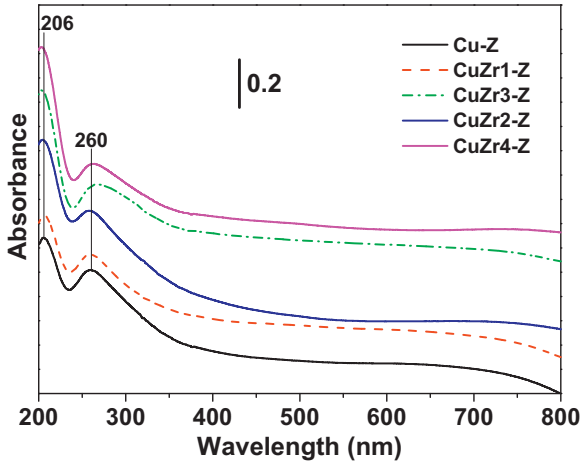

Fig. 10. UV–vis DR spectra of Cu-Z and CuZr-Z catalysts.

Table 3
Redox properties of Cu-Z and CuZr-Z catalysts.

Sample	α peak		β peak		γ peak		δ peak		Total uptake (μmol/g_{cat})
	T (°C)	H_2 uptake (μmol/g_{cat})	T (°C)	H_2 uptake (μmol/g_{cat})	T (°C)	H_2 uptake (μmol/g_{cat})	T (°C)	H_2 uptake (μmol/g_{cat})	
Cu-Z	227	52.1	283	114.5	–	–	–	–	166.6
CuZr1-Z	226	18.4	261	137.2	201	19.8	337	36.6	212.0
CuZr2-Z	230	34.3	278	118.5	198	23.4	334	35.3	211.4
CuZr3-Z	225	25.0	265	136.9	195	9.4	341	40.2	211.5
CuZr4-Z	222	42.9	259	89.9	194	11.1	336	72.1	215.8

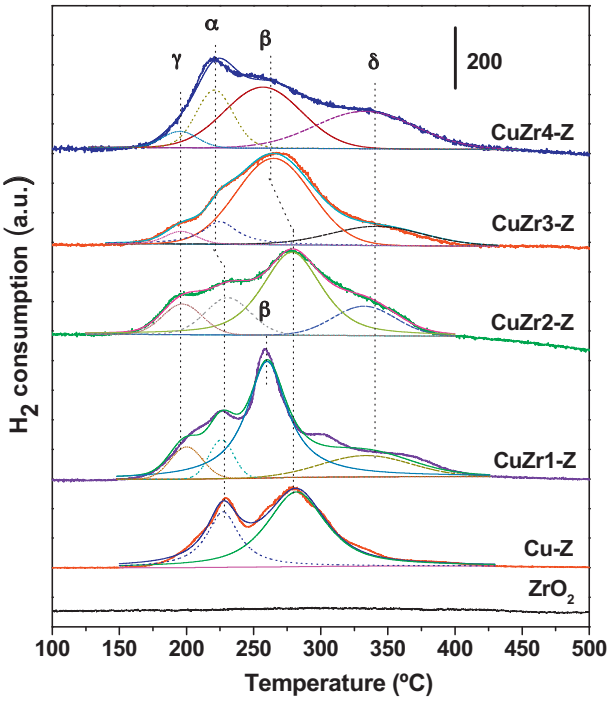

Fig. 11. H_2-TPR profiles of ZrO_2, Cu-Z and CuZr-Z catalysts. Crude line: original data; Smooth line: fitting line. Weight of catalyst: 100 mg; Pretreatment: 20 vol% O_2 at 550 °C for 30 min; Measurement conditions: 10 vol% H_2 (50 mL/min), heating rate 10 °C/min from 50–500 °C.

3.6. H_2-TPR and OSC analysis

The redox behavior of the Cu-Z and CuZr-Z samples was investigated by H_2-TPR. The hydrogen uptake signal was deconvoluted into several peaks identifying the temperature where the H_2 consumption was maximum. Besides, the area under these peaks was integrated in order to evaluate the total amount of hydrogen required for each reduction step. As shown in Fig. 11 and Table 3, two main reduction peaks are identified in all samples: the α peak (222–230 °C), which generally results from the reduction of copper species dispersed on the ZSM-5 support, and the β peak (259–283 °C), from the copper oxide adhering to the external surface of ZSM-5 crystallites. These oxides aggregate to form crystallites that are too small to be detected by XRD. Upon addition of zirconium, both α and β reduction peaks shift moderately to lower values. Combined with the XPS results, it is reasonable to deduce that these copper species in proximity to the zirconium phase are reduced more easily by hydrogen than those on the pure ZSM-5 support. Moreover, some copper ions are incorporated into the vacant sites of the zirconium oxides to form a coordinated, oxygen-capped surface structure [31], corresponding to the γ peak (194–201 °C) and δ peak (334–341 °C) shown in Fig. 11 and Table 3. The formation of mixed oxides results in coordinative unsaturated species, which increase oxygen mobility. The total amount of H_2 consumed can be observed in Table 3. As expected, the H_2 uptake increases from 166.6 to 215.8 μmol/g_{cat} with increasing the zirconium loading from 0 to 2.2 wt%. Thus, reduction is no longer confined to the surface of the material, but extends deep into its bulk, which may accelerate the reduction process and consume more hydrogen.

The OSC of samples was evaluated at 400 °C by the oxygen pulse technique. As shown in Table 4, the OSC for the CuZr-Z sample is considerably higher than that for Cu-Z, which indicates that the combination of copper and zirconium to form composite oxides strongly favors the formation of oxygen vacancies, and thus promotes the migration of oxygen ions. The maximum O_2 uptake is observed for the CuZr3-Z sample with an OSC of 85.5 μmol [O] g^{-1}, followed by CuZr4-Z with an OSC of 73.7 μmol [O] g^{-1}. The OSCs of the used CuZr-Z catalysts are slightly lower than those of the fresh samples. The reason for this may be that the residual nitrate formed during SCR covers the external surface of ZSM-5, limiting oxygen mobility close to oxygen vacancies [32]. Despite this, the OSCs of the used CuZr-Z catalysts are all higher than that of fresh Cu-Z.

3.7. NH_3-TPD analysis

NH_3-TPD profiles of pure ZSM-5, Cu-Z and CuZr-Z samples are shown in Fig. 12. The NH_3-TPD profile of ZSM-5 zeolite displayed two desorption peaks typically seen by using this technique in acidic zeolites [33]. The large desorption profile around 200 °C is ascribed to weakly bound NH_3, which arises from NH_3 physisorbed on Si–OH or from non-zeolitic impurities. The high temperature peak around 415 °C is assigned to NH_3 bound to strong acid sites. Upon introduction of copper and zirconium, the uptake of both weakly and strongly bound NH_3 decreases considerably. The lower amount of NH_3 adsorption in Cu-Z and CuZr-Z samples indicates that the copper and zirconium is unable to bind a significant amount of physisorbed NH_3 [34]. Although the introduction of copper and zirconium leads to a significant decrease in weakly bound NH_3 sites, new bound NH_3 sites are created at 290 and 550–618 °C, respectively. Combined with the finding from XPS that copper and zirconium are enriched on the surface of ZSM-5 grains, it is reasonable to conclude that these stronger acid sites in the range of 550–618 °C mainly originate from metal oxide nanoclusters [35]. NH_3-TPD can give a qualitative indication of acid site strength, but does not differentiate between the Brønsted and Lewis acid sites. In the subsequent section, the DRIFT analysis will address this case.

Table 4
Oxygen storage capacities (OSC) of Cu-Z and CuZr-Z catalysts.

Sample	OSC (μmol [O] g^{-1})	
	Fresh	Used
Cu-Z	9.76	9.64
CuZr1-Z	27.1	26.5
CuZr2-Z	51.8	49.2
CuZr3-Z	85.5	77.2
CuZr4-Z	73.7	71.8

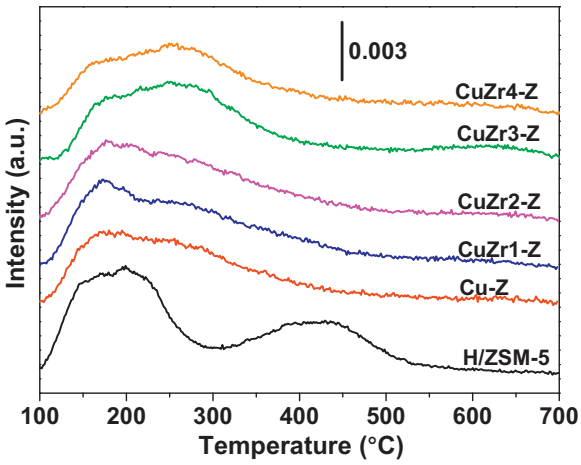

Fig. 12. NH_3-TPD curves of pure ZSM-5, Cu-Z and CuZr-Z catalysts. Weight of catalyst: 100 mg; NH_3 adsorption: 50 °C by pulses of ammonia for 0.5 h; Measurement conditions: He flow: 50 mL/min, heating rate: 10 °C/min from 50–700 °C.

3.8. *In situ* DRIFT analysis

3.8.1. *In situ* DRIFT spectra of NO adsorption

Because of the excellent SCR activity of CuZr3-Z at low temperature, the formation of surface species on CuZr3-Z was probed by *in situ* DRIFT spectroscopy. The sample was exposed to a flow of 1.0 vol% NO + 10 vol% O_2/Ar (40 mL/min) for 30 min, and IR spectra were recorded in succession at 1-min intervals. As shown in Fig. 13A, the adsorption of NO + O_2 for 30 min gave rise to several peaks in the range of 1200–1700 cm^{-1}, where bands indicative of the formation and transformation of adsorbed NO_x species can be analyzed. A negative band at 1257 cm^{-1} could not be clearly distinguished, which is attributed to its masking by a carbonate signal in this region [36]. The assignment of the band at 1354 cm^{-1} is controversial, because various NO_x species show vibration modes in the region between 1300 and 1400 cm^{-1}. Prinetto et al. [37] assigned a band at 1310 cm^{-1} detected during NO adsorption to hyponitrites (NO^-, $N_2O_2^{2-}$). The vibration mode of bridging monodentate nitrites (–N=O) exhibits bands between 1300 and 1450 cm^{-1}, whereas monodentate nitrates are reported to exhibit a band at 1367 cm^{-1} [38,39]. In this study, the band at 1354 cm^{-1} is tentatively assigned to hyponitrites and bridging monodentate nitrites. The weak band at 1380 cm^{-1}, which partially overlaps with the band at 1354 cm^{-1}, is related to weakly adsorbed NO.

Part of the NO adsorbed on the surface copper species exists as bridging and chelating bidentate nitrates, as reflected by the intense asymmetric stretching bands of $-NO_2$ at 1629, 1598 and 1569 cm^{-1} [40]. NO_2 species can be formed as proposed in the literature [41]: the facile reducibility of copper species may easily activate oxygen, which is transferred to NO to form NO_2. Thus, the NO_2 formed is further adsorbed as nitrate intermediate species on the copper sites. We detected NO_2 in this DRIFT experiment, but not in the exhaust during catalytic testing. The uptake of NO_2 by the catalyst to form nitrates may contribute to NO_2 consumption, because it is well known that NO_2 is easily adsorbed by catalysts [42], or it may be consumed during SCR. At higher wavenumber, the bands observed at 1900 and 1803 cm^{-1} are related to the asymmetric and symmetric N–O stretching modes, respectively, of Cu^{2+}–NO and Cu^{+}–NO complexes [38]. This observation indicates that copper exchange into H/ZSM-5 leads to the formation of isolated copper ions. To examine the effect of zirconium addition on adsorbed species, DRIFT spectra of adsorbed NO_x after exposing the Cu-Z catalyst to NO + O_2 were also collected for comparison (Fig. 13B). On close inspection, bands at 1354, 1569, 1598, 1629, 1803 and 1900 cm^{-1} can be observed for the Cu-Z catalyst. The intensities of the bands at 1569, 1598 and 1629 cm^{-1} (adsorbed NO_2 species) are much lower for Cu-Z than those for CuZr3-Z, while the bands at 1803 and 1900 cm^{-1} (adsorbed NO species) remain almost unchanged. These results indicate that the addition of zirconium increases the amount of adsorbed nitrate species formed on the catalyst surface.

3.8.2. *In situ* DRIFT spectra of NH_3 adsorption

To study NH_3 adsorption by DRIFT spectroscopy, the sample was exposed to a flow of 1.0 vol% NH_3 + 10 vol% O_2/Ar (40 mL/min) for 30 min, and IR spectra were recorded in succession at 1-min intervals. The DRIFT spectra of NH_3 + O_2 adsorbed on the CuZr3-Z catalyst are presented in Fig. 13C. The bands at 1294 and 1595 cm^{-1} can be assigned to NH_3 coordinatively adsorbed on Lewis acid sites. The bands at 1467 and 1633 cm^{-1} correspond to the asymmetric and symmetric vibrations of NH_4^+ ions chemisorbed on Brønsted acid sites, respectively. Meanwhile, the band at 1355 cm^{-1} probably originates from the oxidized species of adsorbed ammonia [43]. Shoulder peaks at 1508 and 1569 cm^{-1} are ascribed to amine species (NH_2), while the band at 1432 cm^{-1} is ascribed to imido NH species. Surface NH_2 species can be formed *via* oxidative abstraction of a hydrogen atom from adsorbed ammonia. When more than one hydrogen atom is abstracted from coordinated ammonia, NH species are produced [44]. The shoulder band at 1823 cm^{-1} is caused by weakly adsorbed NH_3. The strong band at 1935 cm^{-1} corresponds to NO species, which arise from the oxidation of adsorbed NH_3. It is worth noting that the band at 1737 cm^{-1} still needs to be assigned. Mouli et al. [45] observed two main bands (1468 and 1730 cm^{-1}) when NH_3 was adsorbed on Ir-Pt/Zr-MCM-41 catalysts, which were assigned to Brønsted acid sites. The same identification was given by Chen et al. [46] for NH_3 adsorbed on V_2O_5-WO_3/TiO_2 catalysts. As such, the absorption peak at 1737 cm^{-1} in our study can be ascribed to NH_4^+ adsorbed on Brønsted acid sites. For comparison, pure ZSM-5 was exposed to NH_3 + O_2 at 170 °C; DRIFT results are shown in Fig. 13D. The ammonia-related bands are similar to those of CuZr3-Z. After the addition of copper and zirconium, the intensity of that bands attributed to Brønsted acid sites (1467 and 1633 cm^{-1}) decrease obviously, whereas the intensity of bands originating from Lewis acid sites (1294 and 1595 cm^{-1}) increase slightly. Correspondingly, the NH_3-TPD results indicate that the introduction of copper and zirconium results in a significant decrease in bound NH_3 sites at 415 °C, but creates new bound NH_3 sites at 290 and 550–618 °C, respectively (Fig. 12). Therefore, we can propose that the decrease of peak at 415 °C can be assigned to NH_3 desorbed from Brønsted acid sites while the creation of new bound NH_3 sites at 290 and 550–618 °C can be attributed to the increase of Lewis acid sites. The reduction in the number of Brønsted acid sites may be because some copper ions are exchanged on the Brønsted acid sites, or because copper and zirconium are enriched on the ZSM-5 surface (as confirmed by the XPS results), which prevent NH_3 from interacting with Brønsted acid sites. The increase in the number of Lewis acid sites is closely related to the increased amount of metal oxide nanoclusters.

3.8.3. *In situ* DRIFT spectra of the reaction between NH_3 + O_2 and adsorbed NO_x species

The CuZr3-Z sample was first treated with 1.0 vol% NO + 10 vol% O_2/Ar (40 mL/min) for 30 min. After purging with Ar, 1.0 vol% NH_3 + 10 vol% O_2/Ar was then introduced into the IR cell, and IR spectra were recorded in succession at 1-min intervals. Fig. 14A shows the DRIFT spectra of the reaction between NH_3 + O_2 and preadsorbed NO_x species on the CuZr3-Z catalyst at 170 °C. After preadsorption of NO + O_2 and purging with Ar, the catalyst surface is mainly covered by three kinds of nitrate ($-NO_2$) species

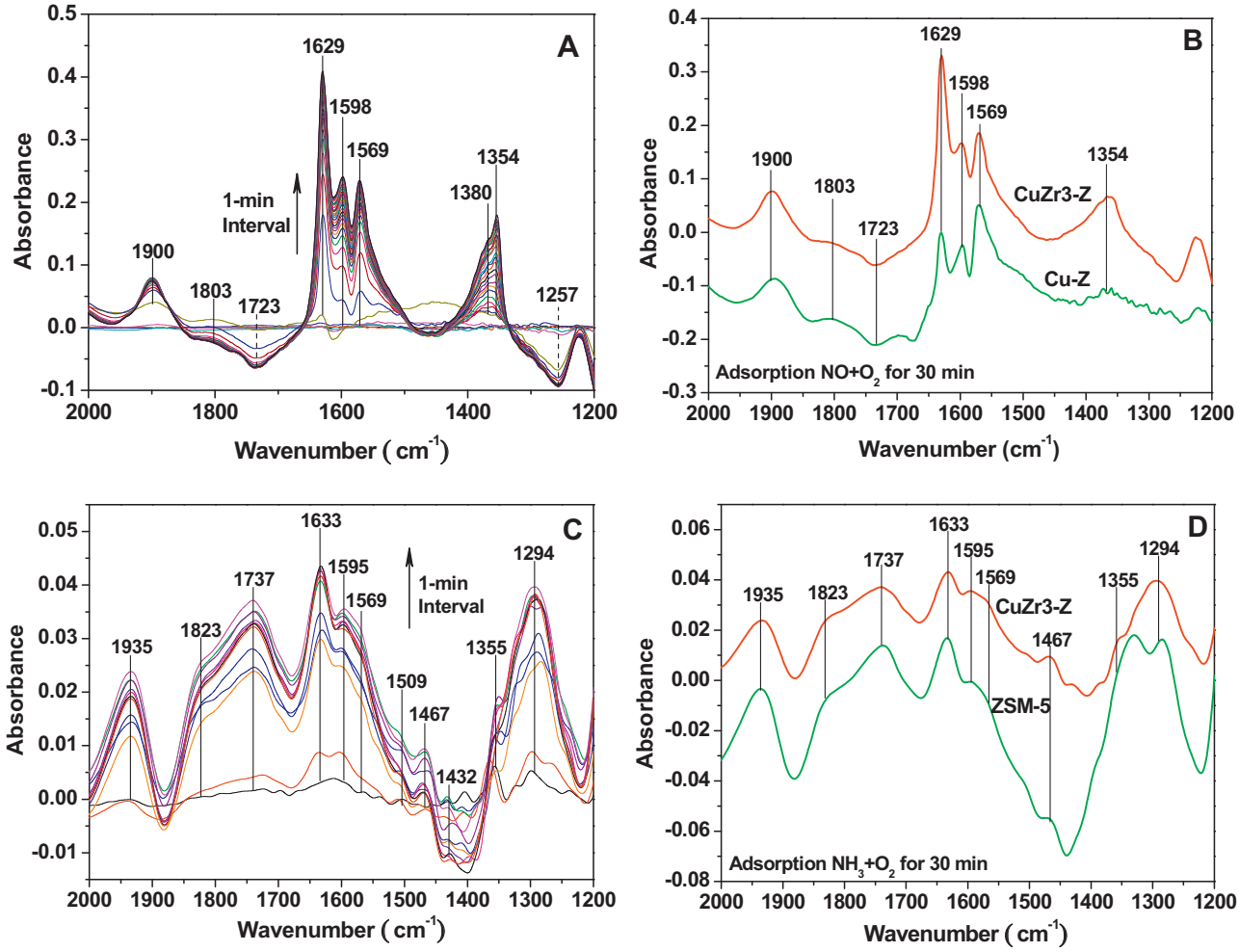

Fig. 13. DRIFT spectra of the CuZr3-Z catalyst arising from NO + O_2 (A) and NH_3 + O_2 (C) adsorption recorded by 1-min interval, and the comparisons between Cu-Z and CuZr-3 form NO + O_2 (B) and between ZSM-5 and CuZr-3 from NH_3 + O_2 (D) adsorption for 30 min. Conditions: 1.0 vol% NO (A, B), 1.0 vol% NH_3 (C, D), 5 vol% O_2 and Ar to balance; flow rate: 40 mL/min; test temperature: 170 °C; spectrum record: 64-scan accumulation and 4 cm^{-1} resolution.

(1569, 1598 and 1629 cm^{-1}), two kinds of –NO species (1803 and 1900 cm^{-1}), and hyponitrites and bridging monodentate nitrites (1354 cm^{-1}). As noted in Fig. 14A, when NH_3 + O_2 is passed over the NO + O_2-preadsorbed CuZr3-Z catalyst, the rapid disappearance of –NO and $–NO_2$ species is observed, implying that these species are very active on the catalyst surface and can quickly react with NH_3. In contrast, the band at 1354 cm^{-1} is observed on the catalyst surface even after NH_3 + O_2 is passed over the catalyst for 30 min, showing that these species are inactive in SCR once formed. Simultaneously, the bands originating from NH_3 adsorption species, *i.e.*, the bands located at 1289 and 1594 cm^{-1} corresponding to Lewis acid sites and the bands located at 1470, 1625 and 1741 cm^{-1} corresponding to Brønsted acid sites, begin to increase in intensity. The presence of a weak band at 1931 cm^{-1} corresponding to –NO species [47] suggests that a side-reaction occurs between NH_3 and O_2, which was also observed in the catalytic activity test. Although the adsorbed NH_3 + O_2 react together, the rate of this reaction is much slower than that between NO + O_2 and NH_3. It is clear that the reaction of NO + O_2 + NH_3 is the main reaction in this system.

3.8.4. *In situ DRIFT study of the reaction between NO + O_2 and adsorbed NH_3 species*

To study the reaction between NO + O_2 and adsorbed NH_3 species, the CuZr3-Z sample was firstly treated with 1.0 vol% NH_3 + 10 vol% O_2/Ar (40 mL/min) for 30 min. After purging with Ar, 1.0 vol% NO + 10 vol% O_2/Ar was then introduced into the IR cell, and IR spectra were recorded in succession at 1-min intervals. Fig. 14B shows the DRIFT spectra of the reaction between NO + O_2 and preadsorbed NH_3 species on the CuZr3-Z catalyst. When NO + O_2 is exposed to NH_3 species adsorbed on CuZr3-Z, the DRIFT spectra clearly show that the NH_4^+ ions at Brønsted acid sites (1470, 1610 and 1738 cm^{-1}) and the NH_3 species adsorbed on Lewis acid sites (1598 and 1288 cm^{-1}) are consumed. This phenomenon suggests that both types of acid sites are involved in the NH_3-SCR reaction. At the same time, some new bands are found on the CuZr3-Z surface, which are ascribed to bridging and chelating bidentate nitrates (1629, 1610 and 1569 cm^{-1}), and weakly adsorbed NO (1803 and 1897 cm^{-1}).

3.8.5. *Proposed reaction pathway*

It is widely accepted that in a typical heterogeneous catalytic reaction, the adsorption of reactants and the activation of adsorbed species are both required for the process to occur. Our *in situ* DRIFT study suggests that the SCR reaction over CuZr3-Z catalyst mainly follows the Langmuir–Hinshelwood mechanism, *i.e.*, reaction of activated NO_x species with activated NH_3 species. The adsorption of NO + O_2 on the CuZr3-Z catalyst reveals the formation of intermediate Cu^{n+}–NO species (n = 1, 2) on ion-exchange sites, and bridging and chelating bidentate nitrates (as reflected by the asymmetric stretch of $–NO_2$) on the CuO_x surface. Bidentate nitrate adsorbates

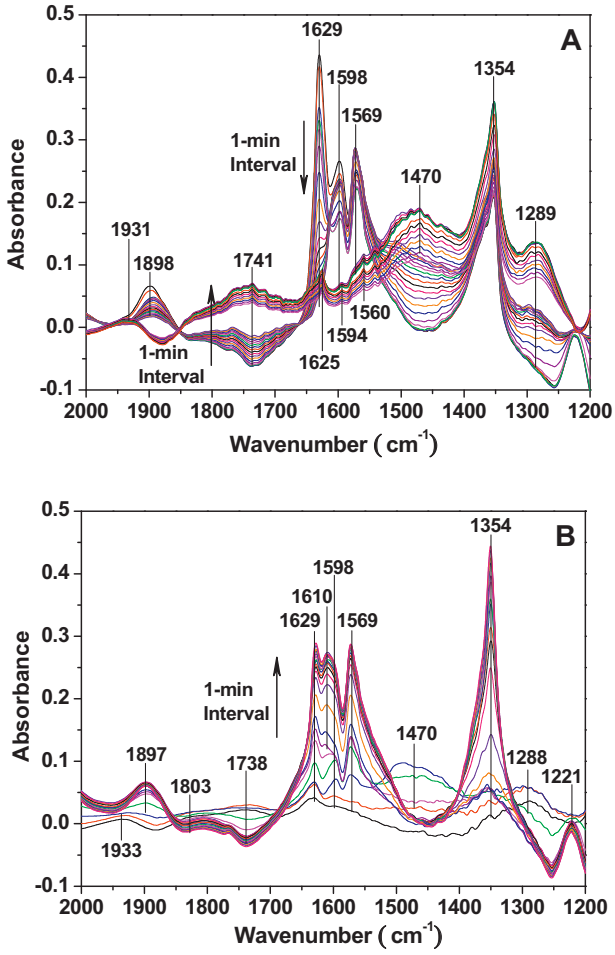

Fig. 14. DRIFT spectra of the reaction between NH_3 and pre-adsorbed NO_x species (A), and between NO_x and pre-adsorbed NH_3 species (B) on the CuZr3-Z catalyst at 170 °C for 30 min. Conditions: 1.0 vol% NO, 1.0 vol% NH_3, 5 vol% O_2 and Ar to balance; flow rate: 40 mL/min; test temperature: 170 °C; spectrum record: 64-scan accumulation and 4 cm^{-1} resolution.

are produced from oxidative adsorption of NO to NO_2 by oxygen bound to copper and subsequent coordination to zirconium at adjacent surface sites. Although this step is accompanied by the reduction of Cu^{2+} to Cu^{+} (that some Cu^{2+} ions are reduced to Cu^{+} was confirmed in Section 3.4), reoxidation should be easily accomplished by oxygen equilibration with the gas phase during NO + O_2 adsorption. The NH_3 species adsorbed on the CuZr3-Z catalyst are present in two forms: protonated NH_3 (NH_4^+) on Brønsted acid sites and coordinated NH_3 on Lewis acid sites. Over the CuZr3-Z catalyst at low temperatures, the reactive nitrates on copper sites react with two neighboring NH_4^+ on Brønsted acid sites to form intermediate species, which further react with gaseous or weakly adsorbed NO (as described in Section 3.7.1) to form N_2 and H_2O. This result is consistent with the mechanism of the "fast SCR" reaction proposed by other authors, where CuO_x clusters catalyze the oxidation of NO to NO_2, which is considered the crucial step affecting performance at low temperature [48,49]. In addition, it is possible that the $-NO_2$ species on copper sites tend to bond with adsorbed NH_4^+ to form NH_4NO_2 species, which behave as an active intermediate in the SCR process. This is the "standard SCR" reaction proposed previously [50,51]. The coordinated NH_3 adsorbed on Lewis acid sites can further undergo oxidative abstraction of hydrogen to yield surface amine ($-NH_2$) species. The $-NH_2$ species subsequently react with –NO species to form NH_2NO intermediate species, which have low thermal stability and easily decompose into N_2 and H_2O. Because of the low thermal stability and rapid decomposition of NH_2NO into N_2 and H_2O, no infrared band attributed to NH_2NO was observed on the catalyst surface under the conditions for SCR [48].

4. Conclusions

The present study highlighted the effects of incorporation of zirconium into Cu/ZSM-5 on SCR activity in NO_x abatement. Addition of zirconium considerably increases the activity of Cu/ZSM-5 for SCR and sulfur tolerance. The Cu-Zr/ZSM-5 catalysts exhibited nearly 100% NO_x conversion over a wide temperature range (167–452 °C), which is markedly superior to those of Cu/ZSM-5 (197–404 °C) and conventional V-W/TiO_2 catalyst (320–450 °C). At least two types of copper species are active in the SCR of NO_x, including isolated copper cations and copper oxide clusters. Addition of zirconium increases the activity of Cu/ZSM-5 for the following reasons:

Firstly, introduction of zirconium increases copper dispersion and inhibits copper crystallization. No diffraction peaks from copper/zirconium oxides were observed in XRD patterns after addition of zirconium, although the intensity of the principal diffraction peaks from ZSM-5 decreased with zirconium content. TEM and UV–vis DR results showed that small copper and zirconium species formed mixed oxide clusters. Some large aggregates of micrometer size were detected when the zirconium content was increased to 1.1 wt%. The inhibition of copper crystallization formed helps to prevent NH_3 oxidation and widen the activity window of the catalyst in the high temperature range.

Secondly, the finely dispersed copper species are enriched on the surface of the ZSM-5 grains. The nitrogen adsorption experiments revealed a decrease of both the BET surface area and micropore volume as the zirconium content increased, indicating that copper and zirconium species cover the surface of ZSM-5 and partially block zeolite channels. It is evident that as the zirconium content increases, the BET surface areas and micropore volumes are inversely related to catalytic performance. According to the XPS results, the catalysts show a steady increase in Cu/Si and Zr/Si surface atomic ratios with zirconium loading. This can explain the higher low-temperature activity observed for the CuZr3-Z catalyst, because it has more exposed copper than the Cu-Z, CuZr1-Z and CuZr-2 catalysts, which facilitates the transfer of energy and mass during SCR.

Thirdly, redox properties seem to play an important role in the SCR of NO_x. H_2-TPR results show that upon addition of zirconium, both α and β reduction peaks shift moderately to lower temperature and their intensities increase. This is because of the higher valence of copper and mobility of lattice oxygen over the CuZr-Z catalysts than over the Cu-Z one. The XPS and OSC results reveal steady increases in surface Cu^{2+}/Cu^{+} and Oo/Oz atomic ratios, as well as OSC values, with zirconium loading. The high OSC and oxygen mobility of the CuZr-Z catalysts with zirconium oxides mean that copper can maintain a high oxidation state even though copper is well dispersed in these catalysts.

Finally, the addition of zirconium promotes the formation of NO_2. The oxidation of NO to NO_2 is thermodynamically favored at low temperature, but it is kinetically restricted. The DRIFT results prove that the CuZr-Z catalysts are able to accelerate the oxidation of NO to NO_2 in the presence of oxygen compared with the Cu-Z catalyst. The increase of $-NO_2$ species induced by zirconium doping facilitates the SCR reaction at low temperatures, which results in the temperature range for optimum NO reduction (>95%) extending to lower values.

Overall, the CuZr-Z catalysts show higher activity toward NO_x reduction than Cu-Z and conventional V-W/TiO_2, obtaining a wide

activity window (167–452 °C) that is within the range of diesel exhaust temperatures.

Acknowledgements

We acknowledge financial support from the National Natural Science Foundation of China (No. 51176139), the National Key Basic Research and Development Program (2013CB228506) and the China Postdoctoral Science Foundation Project (2012T50228).

References

[1] Z. Chen, Q. Yang, H. Li, X. Li, L. Wang, S. Chi Tsang, Journal of Catalysis 276 (2010) 56–65.
[2] L. Sui, L. Yu, Chemical Engineering Journal 142 (2008) 327–330.
[3] L. Čapek, K. Novoveská, Z. Sobalik, B. Wichterlová, L. Cider, E. Jobson, Applied Catalysis B: Environmental 60 (2005) 201–210.
[4] Z. Chajar, M. Primet, H. Praliaud, M. Chevrier, C. Gauthier, F. Mathis, Catalysis Letter 28 (1994) 33–40.
[5] J.L. De Lucas, F. Valverde, A. Dorado, I. Romero, Asencio, Journal of Molecular Catalysis A: Chemical 225 (2005) 47–58.
[6] J.H. Park, H.J. Park, J.H. Baik, I.S. Nam, C.H. Shin, J.H. Lee, B.K. Cho, S.H. Oh, Journal of Catalysis 240 (2006) 47–57.
[7] P.O. Thevenin, A. Alcalde, L.J. Pettersson, S.G. Jaras, J.L.G. Fierro, Journal of Catalysis 215 (2003) 78–86.
[8] R. Zhang, W.Y. Teoh, R. Amal, B. Chen, S. Kaliaguine, Journal of Catalysis 272 (2010) 210–219.
[9] Q. Wang, J.H. Sohn, S.Y. Park, J.S. Choi, J.Y. Lee, J.S. Chung, Journal of Industrial and Engineering Chemistry 16 (2010) 68–73.
[10] V.G. Milt, E.D. Banús, M.A. Ulla, E.E. Miró, Catalysis Today 133–135 (2008) 435–440.
[11] W. Cha, H.A. Le, S. Chin, M. Kim, H. Jung, S.T. Yun, J. Jurng, Materials Research Bulletin 48 (2013) 4415–4418.
[12] C.H. Lin, H. Bai, Industrial & Engineering Chemistry Research 43 (2004) 5983–5988.
[13] M.A.L. Vargas, M. Casanova, A.T.G. Busca, Applied Catalysis B: Environmental 75 (2007) 303–311.
[14] H. Bosch, F. Janssen, Catalysis Today 2 (1988) 369–379.
[15] J. Yu, F. Guo, Y.L. Wang, J.H. Zhu, Y.Y. Liu, F.B. Su, Applied Catalysis B: Environmental 95 (2010) 160–168.
[16] W.S. Kijlstra, M. Biervliet, E.K. Poels, A. Bliek, Applied Catalysis B: Environmental 16 (1998) 327–337.
[17] A.M. Azad, M.J. Duran, A.K. McCoy, M.A. Abraham, Applied Catalysis A: General 332 (2007) 225–236.
[18] P. Bazin, O. Saur, F.C. Meunier, M. Daturi, J.C. Lavalley, A.M. Le Govic, V. Harle, G. Blanchard, Applied Catalysis B: Environmental 90 (2009) 368–379.
[19] C. Montes de Correa, F. Córdoba Castrillón, Journal of Molecular Catalysis A: Chemical 228 (2005) 267–273.
[20] Z. Wu, R. Jin, Y. Liu, H. Wang, Catalysis Communications 9 (2008) 2217–2220.
[21] I.C. Hwang, D.H. Kim, S.I. Woo, Catalysis Today 44 (1998) 47–55.
[22] S.D. Jones, L.M. Neal, M.L. Everett, G.B. Hoflund, H.E. Hagelin-Weaver, Applied Surface Science 256 (2010) 7345–7353.
[23] L.C. Wang, Q. Liu, M. Chen, Y.M. Liu, Y. Cao, H.Y. He, K.N. Fan, Journal of Physical Chemistry C 111 (2007) 16549–16557.
[24] R. Vaidya, R.J. Simonson, J. Cesarano Iii, D. Dimos, G.P. López, Langmuir 12 (1996) 2830–2836.
[25] F. Gao, E.D. Walter, E.M. Karp, J. Luo, R.G. Tonkyn, J.H. Kwak, C.H.F. János Szanyi, Peden, Journal of Catalysis 300 (2013) 20–29.
[26] S.A. Yashnika, A.V. Salnikova, N.T. Vasenina, V.F. Anufrienkoa, Z.R. Ismagilov, Catalysis Today 197 (2012) 214–227.
[27] X. Zhou, H. Chen, X. Cui, Z. Hua, Y. Chen, Y. Zhu, Y. Song, Y. Gong, J. Shi, Applied Catalysis A: General 451 (2013) 112–119.
[28] C. Liang, X. Li, Z. Qu, M. Tade, S. Liu, Applied Surface Science 258 (2012) 3738–3743.
[29] H. Praliaud, S. Mikhailenko, Z. Chajar, M. Primet, Applied Catalysis B: Environmental 16 (1998) 359–374.
[30] H.T. Zhang, G. Wu, X.H. Chen, Materials Chemistry Physics 101 (2007) 415–422.
[31] G. Deo, I.E. Wachs, Journal of Catalysis 146 (1994) 323–334.
[32] K. Sun, W. Lu, M. Wang, X. Xu, Applied Catalysis A: General 268 (2004) 107–113.
[33] L.R. Gonzalez, F. Hermes, M. Bertmer, E.R. Castellon, A.J. Lopez, U. Simon, Applied Catalysis A: General 328 (2007) 174–182.
[34] A. Sultana, T. Nanbaa, M. Haneda, M. Sasaki, H. Hamada, Applied Catalysis B: Environmental 101 (2010) 61–67.
[35] L. Chemielarz, P. Kuśtrowski, R. Dziembaj, P. Cool, E.F. Vansant, Applied Catalysis B: Environmental 62 (2006) 369–380.
[36] Ch. Sedlmair, K. Seshan, A. Jentys, J.A. Lercher, Journal of Catalysis 214 (2003) 308–316.
[37] F. Prinetto, G. Ghiotti, I. Nova, L. Lietti, E. Tronconi, P. Forzatti, Journal of Physical Chemistry B 105 (2001) 12732–12745.
[38] F. Dorado, A. de Lucas, P.B. García, A. Romero, J.L. Valverde, Applied Catalysis A: General 305 (2006) 189–196.
[39] E. Fridell, M. Skoglundh, B. Westerberg, Journal of Catalysis 183 (1999) 196–209.
[40] W. Shan, F. Liu, H. He, X. Shi, C. Zhang, Applied Catalysis B: Environmental 115–116 (2012) 100–106.
[41] A. Sultana, T. Nanba, M. Haneda, H. Hamada, Catalysis Communications 10 (2009) 1859–1863.
[42] H. Lin, Y. Li, W. Shangguan, Z. Huang, Combustion and Flame 156 (2009) 2063–2070.
[43] G. Ramis, L. Yi, G. Busca, Catalysis Today 28 (2008) 373–380.
[44] Y. Liu, T. Gu, X. Weng, Y. Wang, Z. Wu, H. Wang, Journal of Physical Chemistry C 116 (2012) 16582–16592.
[45] K.C. Mouli, V. Sundaramurthy, A.K. Dalai, Z. Ring, Applied Catalysis A: General 321 (2007) 17–26.
[46] L. Chen, J. Li, M. Ge, Journal of Physical Chemistry C 113 (2009) 21177–21184.
[47] X.M. Chen, X.F. Yang, A. Zhu, C.T. Au, C. Shi, Journal of Molecular Catalysis A: Chemical 312 (2009) 31–39.
[48] F.D. Liu, H. He, C.B. Zhang, W.P. Shan, X.Y. Shi, Catalysis Today 175 (2011) 18–25.
[49] A. Grossale, I. Nova, E. Tronconi, D. Chatterjee, M. Weibel, Journal of Catalysis 256 (2008) 312–322.
[50] T.T. Gu, R.B. Jin, Y. Liu, H.F. Liu, X.L. Weng, Z.B. Wu, Applied Catalysis B: Environmental 129 (2013) 30–38.
[51] A. Grossale, I. Nova, E. Tronconi, D. Chatterjee, M. Weibel, Topics in Catalysis 52 (2009) 1837–1841.